Evaluation of Biological Mechanisms of Quanduzhong Capsule for Treating Osteoporosis by Integrating Untargeted Metabolomics and Network Pharmacology

Fang-Fang Yu[1] Le-Yi Huang[1] Man-Man Li[1] Shi-Wen Cui[2] Jie Yuan[2] Xiao-Feng Li[3] Tong Wu[1*]

[1] State Key Laboratory of New Drug and Pharmaceutical Process, Shanghai Institute of Pharmaceutical Industry, China State Institute of Pharmaceutical Industry Co., Ltd., Shanghai, People's Republic of China
[2] National Advanced Medical Engineering Research Center, China State Institute of Pharmaceutical Industry Co., Ltd., Shanghai, People's Republic of China
[3] Research and Development (R&D) Department, Jiangxi Puzheng Pharmaceutical Co., Ltd., Jian, People's Republic of China

Address for correspondence Tong Wu, PhD, Shanghai Institute of Pharmaceutical Industry, China State Institute of Pharmaceutical Industry Co., Ltd., 285 Gebaini Road, Shanghai 201203, People's Republic of China (e-mail: tongwu88@163.com).

Pharmaceut Fronts 2023;5:e197–e208.

Abstract

Osteoporosis (OP) is a metabolic disease characterized by bone formation and resorption disturbances. Quanduzhong Capsule (QDZC) is a common treatment for OP in China; however, the effective components and metabolites of the drug after oral administration remain largely unknown. This study aims to identify the active components, analyze the metabolite changes, and investigate the underlying mechanism against OP. In the study, ovariectomy-induced rat OP model was established, then treated with QDZC. Alendronate sodium tablets (ASTs) were used as a reference drug. The chemical constituents of QDZC were analyzed by UPLC-QTOF-MS (ultra-performance liquid chromatography coupled with quadrupole time-of-flight mass spectrometry) and network pharmacology. The metabolomics was used to analyze differences in serum metabolites of rats in different groups [Sham, Model, Model + QDZC, and Model + AST] at 4, 8, and 12 weeks. Body weight and bone mineral density (BMD) were assessed. Enzyme-linked immunosorbent assay was used to determine serum levels of Akt, p-Akt, ERK, and p-ERK. Our data suggested 86 different chemicals from QDZC, including nine core compounds. QDZC significantly regulated 25 biomarkers linked to arachidonic acid metabolism and unsaturated fatty acid biosynthesis, and promoted serum expression of Akt, p-Akt, ERK, and p-ERK. QDZC might act by activating PI3K-Akt and MAPK signaling pathways. In addition, QDZC may use arachidonic acid derivatives to inhibit osteoclast generation and bone resorption and enhance calcitriol formation to improve calcium absorption and increase bone mass.

Keywords
- osteoporosis
- Quanduzhong Capsule
- UPLC-QTOF-MS
- network pharmacology
- metabolomics

received
February 8, 2023
accepted
June 14, 2023
article published online
August 3, 2023

DOI https://doi.org/10.1055/s-0043-1771048.
ISSN 2628-5088.

Georg Thieme Verlag KG, Rüdigerstraße 14, 70469 Stuttgart, Germany

Introduction

Osteoporosis (OP) is a common bone metabolism disease resulting in bone fragility and fracture susceptibility.[1] A 2022 epidemiological research report covering 11 provinces and 5,728 people in China found that among postmenopausal women over age 40, the prevalence of OP was 32.5% (95% confidence interval: 30.3–34.7%) and positively correlated with age.[2] Epidemiological studies from 2020 and 2021 clarified that age was closely associated with OP risk, and China has the highest proportion of patients with OP worldwide.[3,4] The 2000 Fifth National Census of China found that 6.96% of the total population was aged 65 years or more. The percentage was expected to be 8.87% in 2010 and 13.5% in 2020. An aging population poses a series of challenges. For example, by 2050, 150 million people are expected to be diagnosed with OP,[5] likely increasing China's future medical and socioeconomic burdens.

Duzhong (DZ) is the dry cortex of *Eucommia ulmoides* Oliv.[6] and recorded in the ancient herbal medicine book Shennong Ben Cao Jing. Quanduzhong Capsule (QDZC) is a modern traditional Chinese medicine preparation recorded in the Pharmacopoeia of the People's Republic of China. Its clinical applications include antihypertension, liver, and kidney nourishment, and anti-OP. The main components in DZ are iridoids, lignans, phenylpropanoids, organic acids, steroids, and terpene.[7–11] However, QDZC's components remained largely unknown, and trace components are usually not captured by traditional methods. Therefore, relevant biomarkers and the drug's efficacy must be evaluated to better understand QDZC's anti-OP mechanisms. This study used ultra-performance liquid chromatography MS^E mode, quadrupole time-of-flight mass spectrometry (UPLC-QTOF-MS), and network pharmacology and metabolism to illustrate QDZC's anti-OP mechanisms.

Material and Methods

Materials and Chemicals

QDZCs (Lot number: 200701) were supplied by Jiangxi Puzheng Pharmaceutical Co., Ltd. (Jiangxi, China). Alendronate sodium tablets (ASTs) were purchased from CSPC Ouyi Pharmaceutical Co., Ltd. (Hebei, China). The reference standard aucubin, catalpol, geniposidic acid, and chlorogenic acid (purity $\geq$ 98%) were purchased from the National Institutes for Food and Drug Control (Beijing, China). Standard isochlorogenic acid A (purity 98%) was purchased from Shanghai Boyun Biotech Co., Ltd. (Shanghai, China); pinoresinol diglucoside, isochlorogenic acid C, neochlorogenic acid, cryptochlorogenic acid, deacetylasperulosidic acid, (−)-syringaresinol di-*O*-glucoside, and asiatic acid (purity $\geq$ 98%) were acquired from Shanghai Standard Technology Co., Ltd (Shanghai, China); chenodeoxycholic acid (CDCA; purity $\geq$ 98%) was purchased from Meyer Chemical Technology Co., Ltd. (Shanghai China). Formic acid (FA) and acetonitrile (ACN) of LC-MS (liquid chromatography-mass spectrometry) grade were purchased from Adamas Reagent (Shanghai, China). Analytical-grade methyl alcohol was purchased from Shanghai Titan. Pure distilled water was from Watson's Water (Guangzhou, China). A Milli-Q water system produced ultrapure water.

Metabolomics Study

Animals

Female bilateral ovariectomy (OVX; Sprague–Dawley) rats (35 weeks, 350 ± 20 g) were obtained from Zhejiang Vital River Laboratory Animal Technology Co., Ltd. (Zhejiang, China) and kept at the National Advanced Medical Engineering Research Center for at least 7 days at 25 ± 2°C, 50 ± 10% humidity, a 12-hour dark–light cycle, and unlimited access to distilled water and sterilized food. All experimental procedures were approved by the Animal Ethical Committee of the Shanghai Institute of Pharmaceutical Industry (SYXK 2019–0027).

The rats were randomly allocated to one of four groups ($n = 8$ per group), including one Sham group and three bilateral (OVX) groups: Model (OVX), QDZC (OVX + QDZC, 1 g/kg/d, 2 times the clinical dose), and AST (OVX + AST, 6 mg/kg/wk) groups. QDZC and AST were orally administered to rats in the OVX + QDZC and OVX + AST groups *after* OVX for 12 weeks. We obtained blood from the rats' ocular venous plexuses at 4, 8, and 12 weeks postadministration. The blood was centrifuged at 5,000 rpm for 10 minutes at 4°C to extract serum and kept at −80°C for metabolomics analysis. We used iNSiGHT VET DXA (Dual-energy X-ray absorptiometry, Osteosys, Korea) to measure the bone mineral density (BMD) of the entire lumbar spine and femur in all live rats at week 8.

Sample Collection and Preparation

Using a Multi-Tube vortexer (Targin VX-II, Beijing Targin Technology Co. Ltd., China), we mixed 100 µL of plasma with 300 µL of methanol before centrifuging at 14,000 rpm for 15 minutes at 4°C. In addition, we collected 5 µL of supernatant for mass spectrometry analysis.

Identical volumes (10 µL) of each plasma sample were pooled to create a quality control (QC) sample, which was analyzed like the other samples. During the analytical run, the QC sample was examined to track the stability of the sequence analysis. Ten QC sample replicates were injected (every 5 injections) throughout the study.

UPLC-QTOF-MS Conditions

A Xevo G2-XS QTOF-MS system (Waters, United Kingdom) with an ESI (electrospray ionization) source was used to conduct the MS study. All collected data were managed via Masslynx v4.1 (Waters, United States). The chromatographic separation was performed at a 0.3 mL/min flow rate at 40°C using a Waters HSS T3 column (2.1 mm, 100 mm, 1.8 m). The binary mobile phase contained water (A) (0.1% FA) and ACN (B).

The metabolomics analysis evaluation gradient became as follows: 0–4 minutes, 15% B; 4–9 minutes, 15–30% B; 9–22 minutes, 30–50% B; 22–27 minutes, 50% B; 27–37 minutes, 50–70% B; 37–39 minutes, 70–100% B; 39–42 minutes, 100% B; 42.1 minutes, 15% B; 42.1–44 minutes, 15% B.

MS spectrometry was conducted as follows. Using a 0.3-second scan period, the mass scan data were detected from 50 to 1,500 Da; the flow rate and temperature of the nitrogen desolvation gas were 600 L/h and 250°C, respectively; the cone gas flow rate and source temperature were 50 L/h and 100°C; the sampling cone voltage was 40 V. The low and high energy modes were 6 V and 25–60 V in MS^E mode. The lock mass compound was leucine enkephalin (LE; 0.2 ng/mL). To achieve accurate mass measurements, LE produced reference ions in both positive and negative ion modes (*m/z* 556.2771 $[M+H]^+$ and *m/z* 554.2615 $[M-H]^-$). QDZC compound analysis was performed using non-real-time mass correction. The metabolomics analysis was performed with real-time mass correction. A solution of sodium formate (0.5 mmol/L HCOONa/50% ACN) at a ratio of (1/9) was used for mass calibration.

Data Acquisition and Processing

All metabolomics data were preprocessed by Progenesis QI 2.0 (Nonlinear Dynamics, Newcastle, United Kingdom). The adduct ions were the same as UNIFI (Waters, United States). Progenesis QI was used for peak peaking, deconvolution, and alignment to generate a data matrix and determine the molecular weight and retention time. Using the EZinfo software (Waters Corporation), principal component analysis (PCA) and orthogonal partial least square-discriminant analysis (PLS-DA) were performed on the data matrix. An analysis of variance was used for result confirmation. Metabolites were identified from the Human Metabolome Database (HMDB) database and filtered by VIP value, *t*-test ($p < 0.05$), and fold change ($FC > 2$).

Study on Network Pharmacology

UPLC-QTOF-MS Research of QDZC

Most of the DZ compounds were collected from references.[9,10,12–18] The compound library contains compounds' names, molecular formulas, accurate molecular weights, and structures. We confirmed the structures using online databases such as PubMed, PubChem, CNKI, Science Direct, Springer Link, and Drugfuture. We ultimately found 286 compounds of DZ.

An exact 1.0 g powder sample of QDZC was weighed, steeped in cold solvent (7.5 mL 50% methanol for 30 minutes), then ultrasonically extracted for an hour. The extract was purified with a membrane pore size 0.22 µm filter, and injected with a 5 µL aliquot for AST analysis. The conditions were the same as given in the section "UPLC-QTOF-MS Conditions." The gradient was: 0–4 minutes, 5% B; 4–10 minutes, 5–15% B; 10–25 minutes, 10–13% B; 25–37 minutes, 13–27% B; 37–45 minutes, 27–90% B; 45–49 minutes, 90% B; 49–50 minutes, 90–5% B; 50–55 minutes, 5% B.[7]

The library and MS data were imported to UNIFI™ software for differentiating by retention time, UV absorption, accurate molecular mass, ions, or neutral loss fragments and references. The retention time ranged from 0 to 55 minutes. The target match tolerance was 5 ppm. The adducts in positive mode were $[M+H]^+$, $[M+Na]^+$, and $[M+K]^+$, and in negative mode were $[M-H]^-$, $[M+HCOO]^-$, and $[M+Cl]^-$.

Gene Selection and Network Generation

We searched five databases and references from 2020 to the present to obtain comprehensive OP targets. Targets were collected from *DrugBank* ($n=235$), *Genecards* ($n=1{,}173$), *OMIM* ($n=11$), *PharmGKB* ($n=12$), and *TTD* ($n=30$); the reference targets were investigated in *Pubmed*, including CNR2, EFNB2, EPHB4, ITGB1, NFE2L2, GSK3B, FOXF2, SIRT3, TSC1, BHLHE40, GSTM1, and TFRCU.[19–29] We identified 1,374 targets related to OP after deleting duplicates. We searched for the 85 DZ targets checked by UNIFI from *ETCM*, *HERB,* and *SwissTargetPrediction*. These databases contained 53 compounds linked with 334 targets. Every target was transformed into a gene symbol using the Uniprot station.

We analyzed multiple proteins' STRING database functions as OP and DZ targets. We set the species as homo sapiens and confidence at 0.3 and clicked five times on the more button. We used Cytoscape to determine protein–protein interactions (PPIs) and compound–target networks. We used the CytoNCA plugin to calculate degree, betweenness, and closeness values. The nine core compounds were filtered by the degree values >10 when closeness was the top 15. The core targets' degrees related to the nine compounds were >3. The notes in the compound–target network were ranked by betweenness value. DAVID (Database for Annotation, Visualization and Integrated Discovery, https://david-d.ncifcrf.gov, ver. 6.8) station was used for pathway enrichment.

Biological Verification

According to the manufacturer's instructions, rat Akt, p-Akt, ERK, p-ERK, and estrogen receptor (ER) using enzyme-linked immunosorbent assay (ELISA; R&D Systems Inc., United States) were tested at weeks 4 and 8 using the following procedure: prewarm all reagents to room temperature before assay. Add 100 µL standard or sample to the wells, mix well, and incubate for 20 minutes at 37°C. Wash the plate five times. Add 100 µL enzyme conjugate and wait for 10 minutes at 37°C. Wash plate. Add 100 µL TMB solution and wait for 15 minutes in the dark. Add a stop solution to each well. Assay the optical density at 450 nm using a microplate reader (DENLEY DRAGON Wellscan MK 3, Thermo, Finland) within 30 minutes.

Statistical Analysis

A two-tailed *t*-test was used for analysis, and all outcomes were reported as means ± standard deviation. *p*-Values ≤0.05 were considered statistically significant.

Results and Discussion

Pharmacodynamic Index

Results of the Body Weight and BMD of OVX Rats

Body weights of rats in different groups were measured at 4, 8, and 12 weeks, and shown in ►**Fig. 1A**. Model group's body

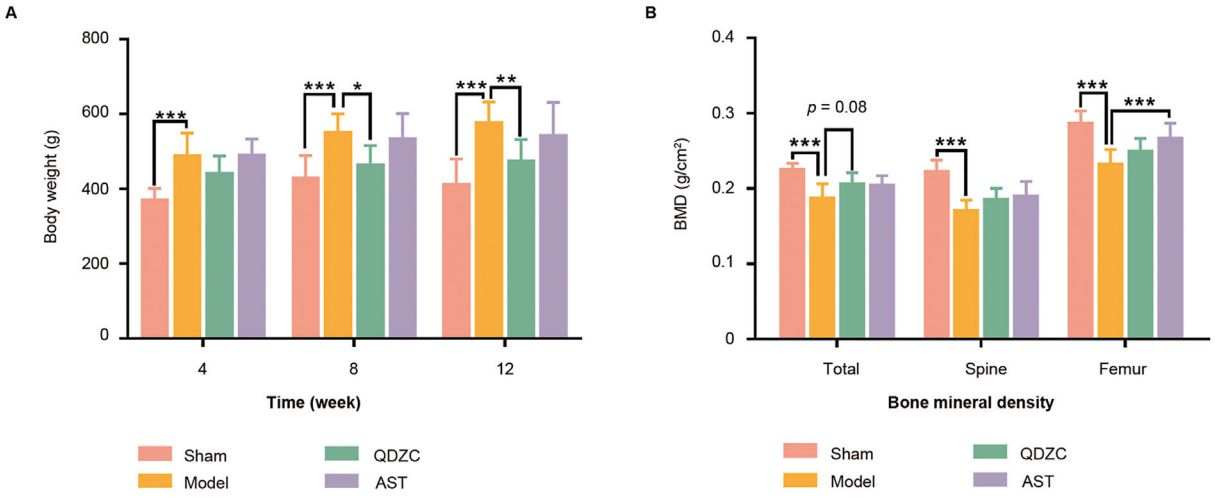

Fig. 1 Impact of QDZC on (**A**) body weight and (**B**) BMD of OVX rats ($n = 7–8$ per group). $^{*}p < 0.05$, $^{**}p < 0.01$, $^{***}p < 0.001$. BMD, bone mineral density; OVX, ovariectomy; QDZC, Quanduzhong Capsule.

weight was significantly higher than the Sham group at 4, 8, and 12 weeks, confirming a weight gain induced by the OVX. However, OVX-induced the weight gain was significantly reversed by additional QDZC treatment. Meanwhile, AST produced same change trend as QDZC, yet, its effect was weaker than QDZC.

BMD values of total, lumbar, and femoral were tested at week 8. As shown in ►**Fig. 1B**, BMD values of Model and treated groups was lower than the Sham group. In addition, BMD values of the treated groups was marginally higher than the Model group, suggesting that QDZC could increase total, spine and femur BMD in rats after 8 weeks of administration.

Metabolomics Study

Metabolite Profiling

We obtained mass spectrum profiles for each group in positive and negative modes after 4, 8, and 12 weeks of administration (►**Fig. 2**). By week 8, the first half signal strength of the QDZC group (H) was significantly different from the Model group (G), which was pulled back to the Sham group (F).

Multivariate Data Analysis

MS data processing and multivariate statistical analyses were conducted by QI software (Waters, Milford, MA,

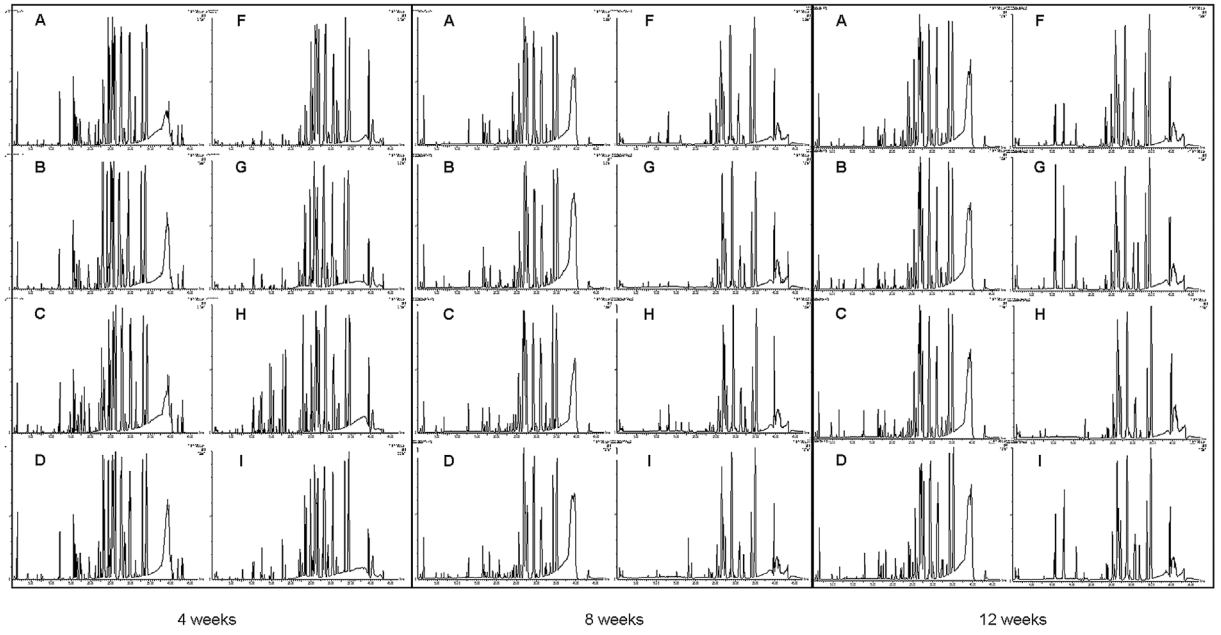

Fig. 2 Metabolite mass spectrum profile of each group at week 4, 8, and 12. Positive mode: (**A**) Sham group, (**B**) Model group, (**C**) QDZC group, (**D**) AST group. Negative mode: (**F**) Sham group, (**G**) Model group, (**H**) QDZC group, (**I**) AST group. AST, alendronate sodium tablet; QDZC, Quanduzhong Capsule.

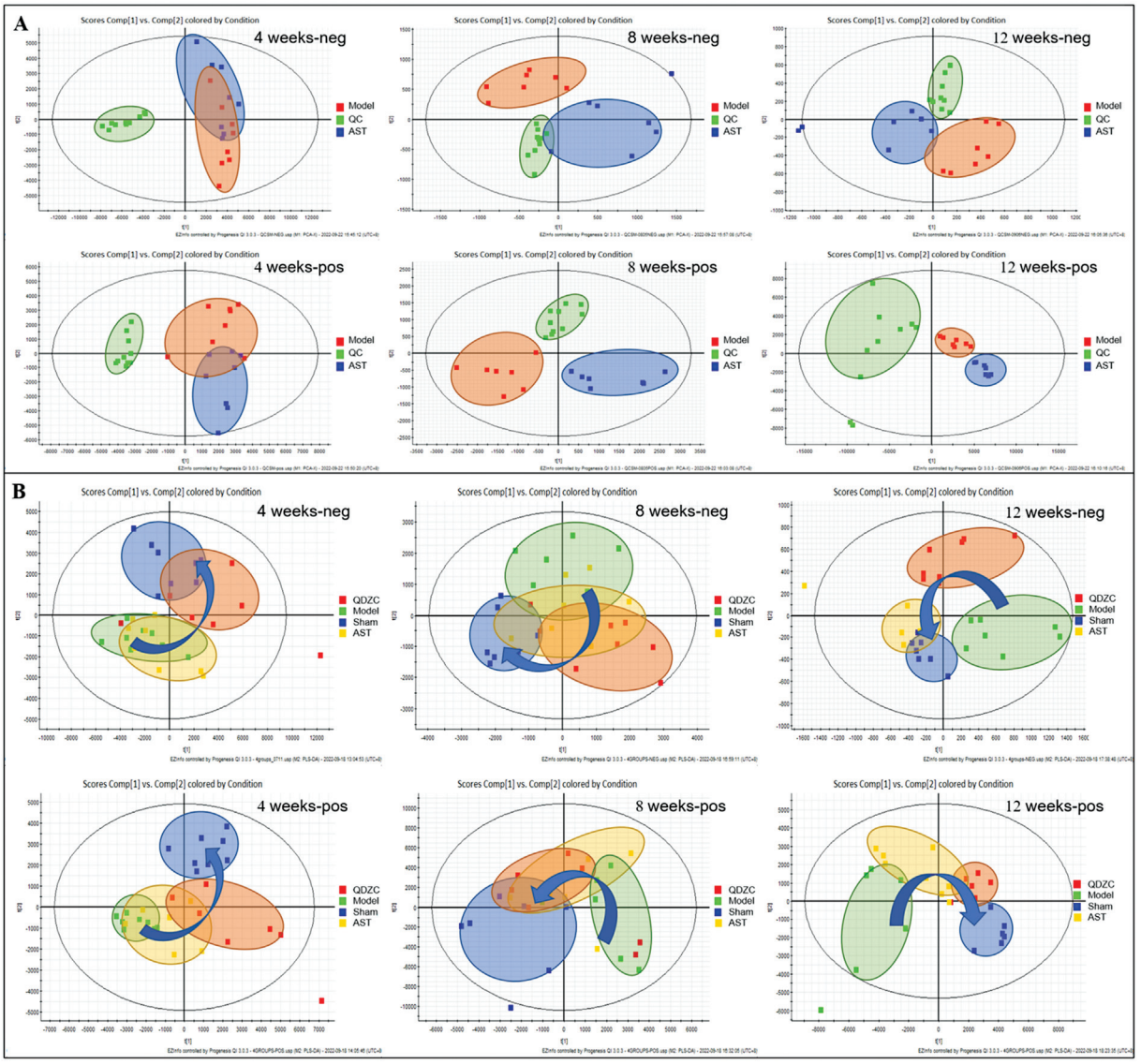

Fig. 3 (**A**) PCA score plot of the MS^E data of Model (*red*), QC (*green*), and Sham (*blue*) groups at week 4, 8, and 12. (**B**) PLS-DA score plot of the MS^E data of QDZC (*red*), Model (*green*), Sham (*blue*), and AST (*yellow*) groups at week 4, 8, and 12. PCA, principal component analysis; PLS-DA, partial least square-discriminant analysis; QDZC, Quanduzhong Capsule.

United States). The PCA diagrams of the Model and Sham groups and QC after 4, 8, and 12 weeks of administration are shown in ►**Fig. 3A**. QC samples were centralized, confirmation of good instrumental stability. In addition, a separation trend between the Sham and Model groups was found while some data portions overlapped. After administration for 8 and 12 weeks, the Sham and Model groups showed significant separation, indicating that different metabolites were generated by the two groups.

PLS-DA models of Sham, Model, QDZC, and AST groups (►**Fig. 3B**) suggested that the plasma metabolite-related OP was positively regulated by the QDZC and AST groups. The AST group appeared similar to the Model group at week 4; however, by week 12, it differed from the Model group and resembled the Sham group. These results suggest that long-term AST administration is indicated in patients with OP. On the other hand, QDZC differed from the Model group (and appeared closer to the Sham group) at three time points. These results suggest that QDZC effectively treated OP. Nevertheless, it was necessary to further analyze the changes of metabolites *in vivo* caused by QDZC during OP treatment and predict its mechanism of action.

Potential Biomarker and Biological Significance

Metabolites and their trends are shown in ►**Tables 1**, **2**, and **3**. A total of 25 biomarkers were identified over three administration cycles by comparing the HMDB database (https://hmdb.ca/) and mass spectrum fragmentation information. Most of these endogenous metabolites were phosphatidylcholines, sterols, unsaturated fatty acids, and bile acids, suggesting that QDZC treated OP through different metabolic pathways. The eight common metabolites identified at weeks 4 and 8 were phosphatidylcholines. In addition, there were nine common metabolites—including phosphatidylcholines, CDCA, and

Table 1 Metabolites and their trends between Sham and Model or QDZC and Model of three administration cycles

No.	Compound ID	RT (min)	Description	Sham vs. Model	QDZC vs. Model	Time (wk)
M1	HMDB0030964	38.06	Linolenelaidic acid	↑#	↑*	4
M2	HMDB0255576	3.210	Nialamide	↑	↑*	4
M3	HMDB0062656	36.25	Linoleamide	↑	↑	4
M4	HMDB0001043	39.47	Arachidonic acid	↑##	↑**	4
M5	HMDB0013039	12.96	Prostaglandin G1	↑##	↓	8
M6	HMDB0000747	19.45	Isovalerylalanine	↓###	↓	8
M7	HMDB0035440	28.59	α, β-Dihydroxanthohumol	↓###	↓***	8
M8	HMDB0004673	32.11	11,12-Epoxyeicosatrienoic acid	↑	↑**	8
M9	HMDB0000207	33.66	Oleic acid	↓###	↓***	8
M10	HMDB0000569	6.250	Deoxypyridinoline	↓###	↓***	12
M11	HMDB0005082	6.920	Lipoxin B4	↑#	↑*	12
M12	HMDB0304121	8.280	3-Dehydrocholate	↓**	↓**	12
M13	HMDB0031900	6.250	Methyl (2*E*,4*Z*,6*E*,8*E*,10*E*)-4,8 -dimethyl-12-oxo-2,4,6,8, 10-dodecapentaenoate	↓###	↓***	12

Note: $^{\#}p<0.05$, $^{\#\#}p<0.01$, $^{\#\#\#}p<0.001$ vs. Sham group; $^{*}p<0.05$, $^{**}p<0.01$, $^{***}p<0.001$ versus Model group.

Table 2 Eight common metabolites at week 4 and 8, or week 8 and 12

No.	Compound ID	RT (min)	Description	Sham vs. Model group		QDZC vs. Model group	
				4 wk	8 wk	4 wk	8 wk
M14	HMDB0010384	36.69	LysoPC (18:0/0:0)	↑	↑##	↑	↑**
M15	HMDB0012108	32.37	LysoPC (17:0/0:0)	↓	↑#	↑*	↑**
M16	HMDB0240599	32.50	LysoPE (P-18:1(9*Z*)/0:0)	↓###	↓###	↓***	↓**
				8 wk	*12 wk*	*8 wk*	*12 wk*
M17	HMDB0000518	18.91	Chenodeoxycholic acid	↑##	–	↑	↑**
M18	HMDB0001999	10.05	Eicosapentaenoic acid	↓##	↓	↓***	↓
M19	HMDB0006228	26.99	24-Hydroxycalcitriol	↑	↑#	↑	↑**
M20	HMDB0010392	10.13	LysoPC (20:2(11*Z*, 14*Z*)/0:0)	↑###	↑	↑*	↑*

Note: $^{\#}p<0.05$, $^{\#\#}p<0.01$, $^{\#\#\#}p<0.001$ vs. Sham group; $^{*}p<0.05$, $^{**}p<0.01$, $^{***}p<0.001$ vs. Model group.

Table 3 Nine common metabolites at week 4, 8, and 12

No.	Compound ID	RT (min)	Description	Sham vs. Model group			QDZC vs. Model group		
				4 wk	8 wk	12 wk	4 wk	8 wk	12 wk
M21	HMDB0010381	25.45	LysoPC (15:0/0:0)	↑##	↑##	↑#	↑*	↑*	↑*
M22	HMDB0011490	36.87	LysoPE (0:0/22:0)	↑##	↑##	↑#	↑	↑*	↑*
M23	HMDB0010395	19.84	LysoPC (20:4(5*Z*, 8*Z*, 11*Z*, 14*Z*)/0:0)	↑###	↓##	↑##	↑***	↓**	↑
M24	HMDB0011511	32.37	LysoPE (20:0/0:0)	↓	↑#	↑#	↑*	↑*	↑*
M25	HMDB0258493	36.69	2-Lysophosphatidylcholine	↑	↑##	↑##	↑	↑**	↑**

Note: $^{\#}p<0.05$, $^{\#\#}p<0.01$, $^{\#\#\#}p<0.001$ vs. Sham group; $^{*}p<0.05$, $^{**}p<0.01$, $^{***}p<0.001$ vs. Model group.

24-hydroxycalcitriol (24-HCT)—at weeks 8 and 12. Five phosphatidylcholine metabolites are generally up-regulated after 4, 8, and 12 weeks of administration.

Due to their lack of estrogen, castrated rats exhibit bone loss and bone metabolism disorder symptoms. Estrogen deficiency can stimulate RAKNL expression and extend osteoclasts' lifespans while shortening osteoblasts'.[30] Enrichment analysis of pathways containing 25 differential metabolites revealed five pathways: unsaturated fatty acid biosynthesis, arachidonic acid metabolism, glycerophospholipid metabolism, steroid biosynthesis pathway, and primary bile acid biosynthesis. Only the first two pathways had p-values <0.05 with $-\log(p) > 2$; consequently, arachidonic acid metabolism and unsaturated fatty acid biosynthesis were selected for analysis.

Arachidonic acid plays a key role in arachidonic acid metabolism, and is a precursor for synthesizing prostaglandins, leukotrienes, and thromboxanes. For example, 11,12-epoxyeicosatrienoic acid (11,12-EET), a metabolite of AA catalyzed by CYP4A, reportedly inhibits osteoclast production and bone resorption by reducing the effect of RNAKL on nuclear factor kappa B (NF-κB) activation.[31] EETs simultaneously activate PI3K-Akt and ERK signal transduction and promote ERK phosphorylation,[32] consistent with the increase of Akt and p-ERK concentrations in the Sham and DZ groups according to the ELISA results. In addition, AA and 11,12-EETs were significantly up-regulated compared with the Model group in the Sham and drug administration groups.

Oleic acid, linolenelaidic acid, arachidonic acid, and eicosapentaenoic acid (EPA) participate in the biosynthesis of unsaturated fatty acids. EPA increases the expression of Runx2 and reduces PPARγ to promote the differentiation of mesenchymal stem cells (MSCs) into osteoblasts. Furthermore, EPA can combine with PPARγ in MSCs to inhibit the transcriptional activity of NF-κB, thereby inhibiting osteoclast formation.[33]

24-HCT is a metabolite whose content increased in the blood sample at weeks 8 and 12, an effect closely related to vitamin D (VD). As a therapeutic drug for treating OP, VD is mainly used to promote intestinal absorption of calcium and advance bone mineralization.[34] VD is metabolized to generate calcifediol and calcitriol and then is transformed into 24-HCT. 24-HCT was significantly up-regulated in the Sham and drug administration groups compared with the Model group. Calcitriol is an active VD and can directly treat OP without activating kidney 1α-hydroxylase. Long-term use of CDCA could increase bone density, likely related to promoting VD absorption.[35] The Sham and QDZC groups had higher CDCA than the Model group. Therefore, QDZC treats OP by enhancing CDCA secretion, increasing VD absorption, increasing calcitriol formation, and promoting intestinal absorption of calcium to increase bone mass.

Different trends in Lipoxin B4 (LXB4), a metabolite closely related to OP, also appeared in week 12. LXB4Z was significantly increased in the Sham and drug administration groups compared with the Model group. Inflammation could promote bone resorption. For instance, tumor necrosis factor-α can help differentiate osteoclast precursors into mature osteoclasts and attract monocytes, thus increasing bone absorption.[36] Lipoxin A4 (LXA4) and LXB4 possess analgesic effects on inflammatory and neuropathic pain, help eliminate proinflammatory factors, and lessen mechanical pain in the spinal cord in patients with late-stage bone cancer. Moreover, LXA4 could interfere with the MAPK signal pathway and inhibit NF-κB and AP-1 expression, thus controlling proinflammatory cytokine release. Additionally, EPA is a precursor for pro-resolving lipid mediators (SPMs). SPMs, also called resolvins, are important for reducing inflammation. As an SPM derived from AA, LXB4 inhibits inflammation by counteracting the proinflammatory effects of leukotriene and prostaglandin and stimulating macrophages to clear apoptotic neutrophils.[37]

Deoxypyridinoline (DPD) is one of the best-characterized bone resorption markers and often appears simultaneously with pyridinoline. The higher the DPD content, the higher the bone resorption level.[38] DPD was much lower in the Sham and administration groups than in the Model groups, suggesting that QDZC could reduce bone resorption.

Network Pharmacology Research

Analysis of QDZC

We analyzed a 50% methanol extract of QDZC using UPLC-QTOF-MS. The data were screened by matching with a self-built database using UNIFI software. As shown in ►**Fig. S1** (in the Supporting Information, available in online version), 86 peaks were detected and tentatively characterized. These peaks comprised 31 lignans, 17 organic acids, 13 iridoids, 2 phenylpropanoids, 2 aldehydes, 1 alcohol, 1 coumarin, 1 ionone, 1 carbohydrate, 1 triterpene, 9 other compounds, and 7 unidentified compounds. Eleven compounds were identified by comparing their retention times, accurate mass-to-charge ratios, and fragment ions with standards. The 86 components are detailed in ►**Table S1** (in the Supporting Information, available in online version).

Network Construction and Pathway Analysis

Nine core compounds and 19 core targets were obtained by screening the PPI network (►**Table S2**, [available in online version]). The "compound–target" network of eucommiol II, madecassic acid, (+)1-hydroxypinoresinol, isochlorogenic acid A, aucubin, neochlorogenic acid, pinoresinol, catalpol, chlorogenic acid, and their related targets is shown in ►**Fig. 4**. We identified an additional 143 pathways by enriching core targets in DAVID. After deleting unrelated pathways—like cancer and bacterial infection—14 pathways (►**Table 4**) with degree values >10 and p-values <0.05 were selected. These pathways could be key pathways of QDZC on OP.

To reflect the targets of compounds on the pathway, we established a compound–target–pathway map (►**Fig. 5**) that displayed the interactions between nine substances on various signaling pathways, including estrogen, PI3K-Akt, MAPK, FoxO, IL-17, Wnt, lipid, and atherosclerosis, and ovarian steroidogenesis signaling pathways. Several compounds

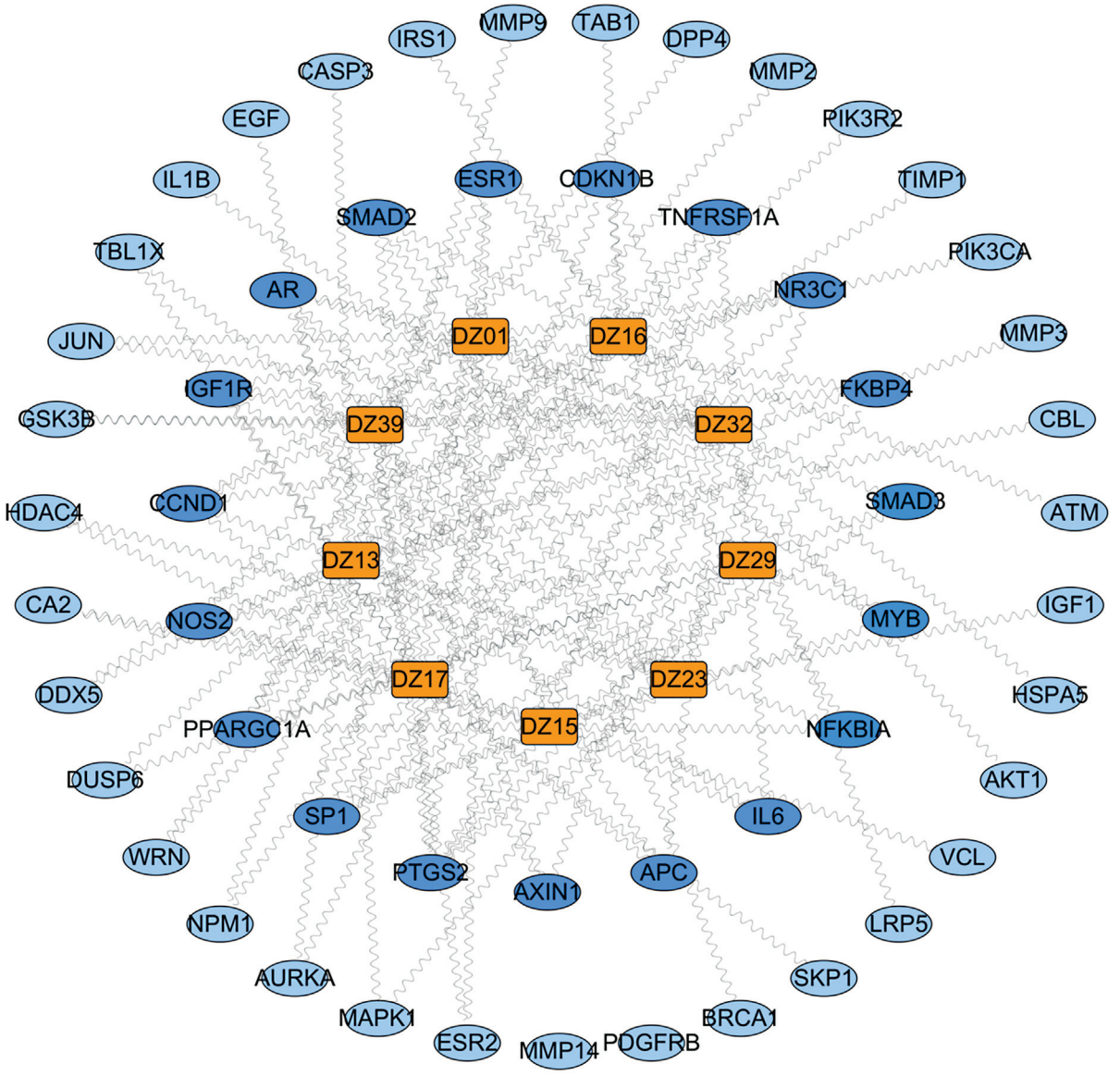

Fig. 4 Component (*orange*): target protein (*blue*) network of QDZC. The *dark blue* is the 19 core targets related to QDZC and OP. DZ01, (+)1-hydroxypinoresinol; DZ13, asiatic acid; DZ15, aucubin; DZ16, catalpol; DZ17, chlorogenic acid; DZ23, eucommiol II; DZ29, isochlorogenic acid A; DZ32, neochlorogenic acid; DZ39, pinoresinol. OP, osteoporosis; QDZC, Quanduzhong Capsule.

affected the targets ER, RTK, ERK, IGF1R, TNFR, IL-6, and IL-1, potential anti-OP targets of QDZC. We selected the PI3K-Akt, MAPK, and estrogen signaling pathways as core pathways for biological verification because most compounds act on targets located on these pathways. Akt and ERK are pathway intersections. Eucommiol II, asiatic acid, and isochlorogenic acid A may act on ERK and appear related to meiosis, mitosis, and anaphase functions. Chen et al[39] reported that ERK promoted the differentiation of osteoblasts from bone marrow stem cells after phosphorylation and prevented further OP-related deterioration.

We used the HMDB database to integrate the results of metabolomics and network pharmacology and identify potential biomarker targets (using the same method as in the section "Gene Selection and Network Generation") to establish the PPI of metabolites. The relationships of metabolites, enzymes, biomarker targets, related pathways, and nine core QDZC compounds are shown in ►**Fig. 6**. The pathways depicted in ►**Fig. 6** comprise overlap between metabolites and compounds, meaning that those components may affect the pathways' metabolic enzymes to up- or down-regulate various biomarkers. For example, pink targets PPARGC1A, NFKBIA, ESR1, SMAD3, NR3C1, and SP1 are shared with the component–target protein network and metabolite–target–compound network, meaning the compound may act on these targets to influence biomarker synthesis or secretion. For example, genetic variations in ESR1 were correlated with BMD.[40] By combining the results of the two networks, we predicted that 1-hydroxypinoresinol, asiatic acid, and

Table 4 Fourteen key pathways of QDZC on osteoporosis

KEGG ID	Pathway	Gene hit
hsa05417	Lipid and atherosclerosis	17
hsa04151	PI3K-Akt signaling pathway	15
hsa01522	Endocrine resistance	14
hsa04010	MAPK signaling pathway	14
hsa04068	FoxO signaling pathway	13
hsa04657	IL-17 signaling pathway	12
hsa04625	C-type lectin receptor signaling pathway	12
hsa04066	HIF-1 signaling pathway	12
hsa04380	Osteoclast differentiation	12
hsa04620	Toll-like receptor signaling pathway	11
hsa04926	Relaxin signaling pathway	11
hsa04915	Estrogen signaling pathway	11
hsa04550	Signaling pathways regulating pluripotency of stem cells	11
hsa04150	mTOR signaling pathway	11

Abbreviation: mTOR, mammalian target of rapamycin.

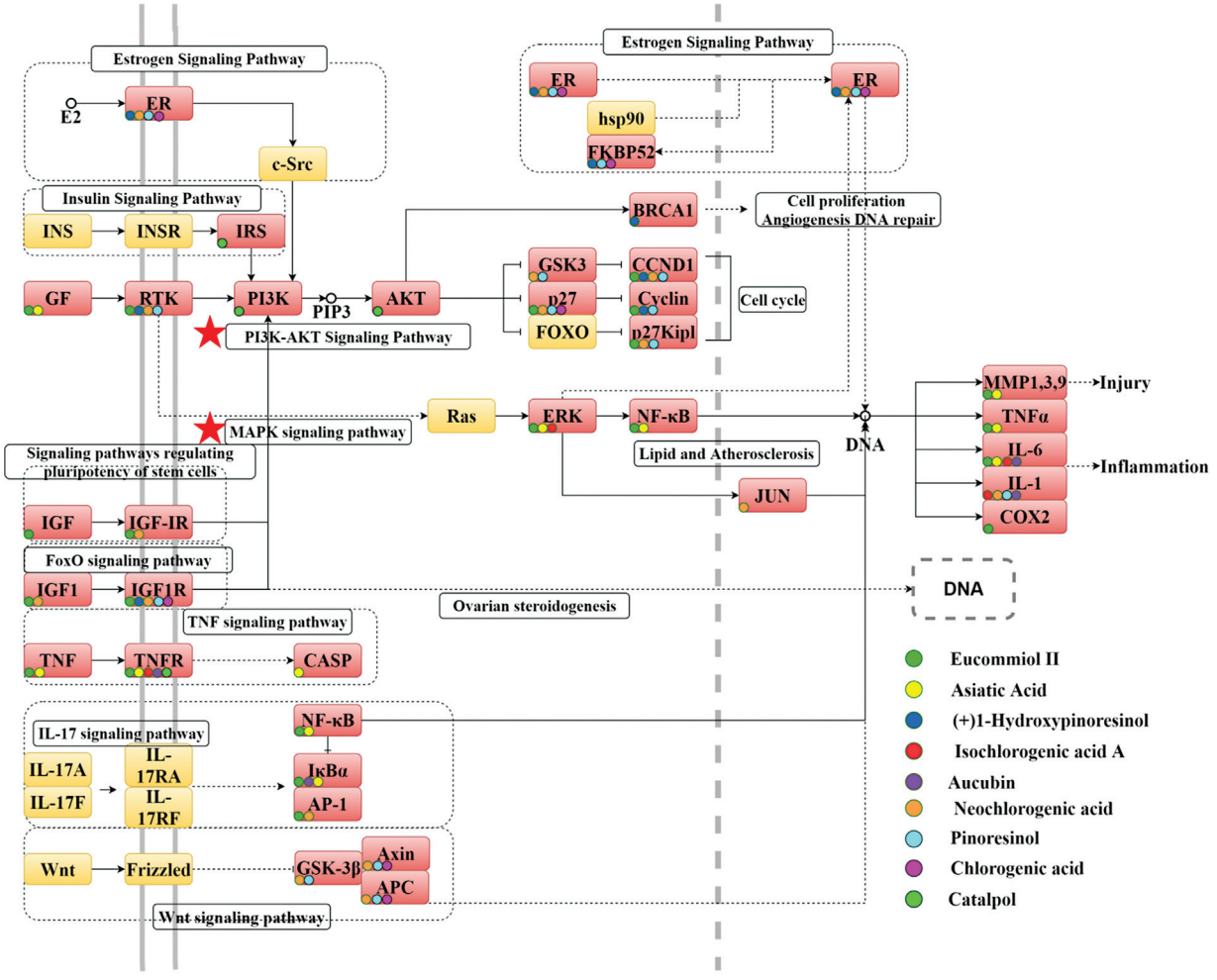

Fig. 5 Compound–target–pathway map of QDZC. The targets that the compound hit are *red*, and none is *yellow*. Text boxes are the pathway labels. QDZC, Quanduzhong Capsule.

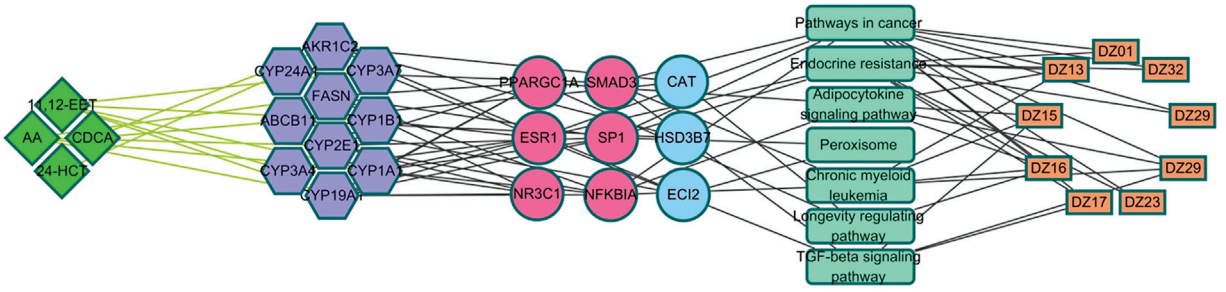

Fig. 6 Metabolite–target–compound network. The meaning of colors and shapes: metabolites (*green*, diamond), enzymes (*purple*, hexagon), targets (*pink* and *blue*, ellipse), pathway (*cyan*, round rectangle), compounds (*orange*, rectangle). The *pink* circle means the core targets are shared with the "compound–target" network.

pinoresinol affected ER expression, potentially changing AA, 24-HCT, 11,12,-EET, or CDCA concentrations.

Biological Verification

According to the ELISA results (►**Fig. 7**), the groups' proteins differed after modeling. Akt and p-Akt expression increased significantly at week 8 compared with week 4. Meanwhile, ERK, p-ERK, and ER remained unchanged. Compared with the Sham group, the Model group's ER expression level was significantly increased at week 4. After 8 weeks of administration, the ER content in the QDZC and AST groups displayed a downward trend compared with the Model group; however, these changes were not statistically significant. Furthermore, the Model group's p-Akt content was higher than the Sham group's ($p < 0.01$) at week 4, while it was lower than the Sham group's at week 8 ($p < 0.05$). The QDZC and the AST groups'

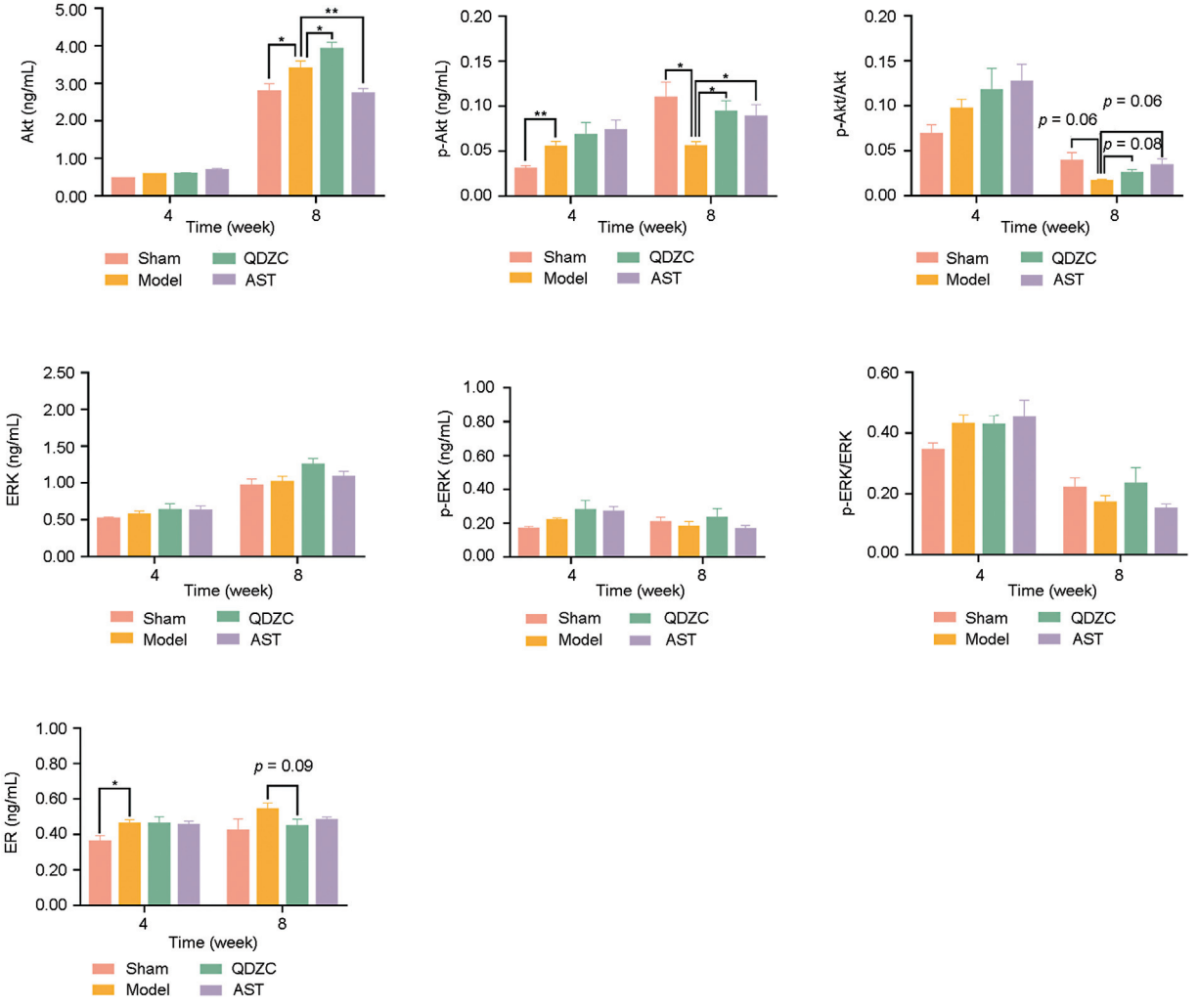

Fig. 7 ELISA analysis demonstrated the expression levels of Akt, p-Akt, ERK, p-ERK, p-Akt/Akt, and p-ERK/ERK in rat plasma. Data were presented as the mean ± SD ($n = 7–8$ per group). ELISA, enzyme-linked immunosorbent assay; SD, standard deviation.

p-Akt were significantly increased ($p < 0.05$) compared with the Model group.

Further confirmatory p-Akt/Akt ratio analyses indicated that QDZC and AST might activate the PI3K/Akt pathway. In addition, the Model group's p-ERK level was lower than the Sham group's after 8 weeks of administration; however, this difference did not rise to the level of statistical difference. The trend of initial increases, followed by decreases, was shown in the p-ERK content of the QDZC and AST groups at weeks 4 and 8, but no statistical differences were observed. ERK levels in the QDZC group were highest at weeks 4 and 8 compared with other groups; similar results were obtained for p-ERK. Although these outcomes did not achieve statistical significance, QDZC may increase ERK and p-ERK levels. Further analysis of the p-ERK/ERK ratio verified this result, indicating that QDZC might also play a protective role by regulating the MAPK pathway. When we integrated the QDZC map and biological target verification, QDZC's protective effects on OP rats appeared related to PI3K/Akt and MAPK pathway regulation.

Conclusion

Bioactive components of QDZC (i.e., eucommiol II, asiatic acid, pinoresinol, (+)1-hydroxypinoresinol, isochlorogenic acid A, aucubin, neochlorogenic acid, chlorogenic acid, and catapol) act on PI3K-AKT and MAPK signaling pathways. We used ELISA to verify increased Akt and ERK expression in the QDZC group and found that QDZC affected PI3K-AKT and MAPK signal pathways. Although we did not observe the up-expression of the ER protein, we could not rule out a connection between QDZC and the estrogen signaling pathway for the network pharmacology and metabolomics results related to ESR1 and the estrogen signaling pathway. Based on the metabonomic analysis, QDZC appears to increase calcium absorption and inhibit bone absorption associated with OP. First, 11,12-EETs and EPA arachidonic acid derivatives inhibited osteoclast formation and bone resorption. PI3K-Akt and ERK signal pathways were activated by EPA to promote ERK phosphorylation and then regulate cell proliferation and differentiation. EPA could also be derived from resolvins to inhibit inflammation and reduce bone absorption.

Second, QDZC might improve bone mass by promoting CDA secretion, increasing calcitriol synthesis, and enhancing calcium absorption. Finally, network pharmacology and metabonomics were used to clarify the mechanism of OP and provide a starting point for future research involving rat models or cellular-level experiments.

Supporting Information

The base peak intensity (BPI) chromatograms of QDZC in negative positive and ion modes; the secondary mass spectra of several representative chemical constituents of *E. ulmoides* and its possible cleavage pathways; the serum BPI chromatograms of QDZC in negative; the chemical constituents of *E. ulmoides* by UHPLC-QTOF-MS in negative and positive ion modes; the nine core compounds and 19 core targets of QDZC identified; as well as the components of QDZC in serum are included in the Supporting Information (►**Figs. S1**, **S2**, **S1.1**–**S1.5**, ►**Tables S1**–**S3** [available in online version]).

Conflict of Interest
None declared.

References

1 Rachner TD, Khosla S, Hofbauer LC. Osteoporosis: now and the future. Lancet 2011;377(9773):1276–1287
2 Tang SS, Yin XJ, Yu W, et al. Prevalence of osteoporosis and related factors in postmenopausal women aged 40 and above in China [in Chinese]. Zhonghua Liu Xing Bing Xue Za Zhi 2022;43(04):509–516
3 Wang YP. Epidemiological Investigation and TCM Syndrome Characteristics of Early Osteoporosis [in Chinese]. Changchun: Changchun University of Chinese Medicine; 2022
4 Zhao JJ, Cao YJ, Sun JX, et al. Prevalence and influencing factors of osteoporosis among adults in Hebei province. [in Chinese]. Chin J Publ Health 2022;38(06):749–751
5 Zhang C, Tan L, Zhu W, Yang Z, Guo M. Research progress on prevention and treatment of osteoporosis by Eucommia ulmoides. International Journal of Clinical and Experimental Medicine Research. 2022;6(03):286–294
6 Chinese Pharmacopoeia Commission. Pharmacopoeia of the People's Republic of China. 2010 ed. Beijing: Chinese Medicine Science and Technology Press; 2010:168–169
7 He M, Jia J, Li J, et al. Application of characteristic ion filtering with ultra-high performance liquid chromatography quadrupole time of flight tandem mass spectrometry for rapid detection and identification of chemical profiling in Eucommia ulmoides Oliv. J Chromatogr A 2018;1554:81–91
8 Huang Q, Tan JB, Zeng XC, Wang YQ, Zou ZX, Ouyang DS. Lignans and phenolic constituents from *Eucommia ulmoides* Oliver. Nat Prod Res 2021;35(20):3376–3383
9 Huang L, Lyu Q, Zheng W, Yang Q, Cao G. Traditional application and modern pharmacological research of Eucommia ulmoides Oliv. Chin Med 2021;16(01):73
10 Wang CY, Tang L, He JW, Li J, Wang YZ. Ethnobotany, phytochemistry and pharmacological properties of Eucommia ulmoides: a review. Am J Chin Med 2019;47(02):259–300
11 Liu P, Wang L, Du Q, Du H. Chemotype classification and biomarker screening of male *Eucommia ulmoides* Oliv. flower core collections using UPLC-QTOF/MS-based non-targeted metabolomics. PeerJ 2020;8:e9786
12 He X, Wang J, Li M, et al. Eucommia ulmoides Oliv.: ethnopharmacology, phytochemistry and pharmacology of an important traditional Chinese medicine. J Ethnopharmacol 2014;151(01):78–92
13 Zhang ZL, Zuo YM, Li YY, Chen LY, Liu RH. Phenylpropanoids constituents of Eucommia ulmoides leaves. [in Chinese]. Zhong Yao Cai 2014;37(03):421–423
14 Li J, Wang M, Wang X, Sun L, Zhao C, Zhao M. Rapid characterization of the chemical constituents of Duzhong Jiangya tablet by HPLC coupled with Fourier transform ion cyclotron resonance mass spectrometry. J Sep Sci 2020;43(24):4434–4460
15 Ding Y, Dou D, Guo Y, Li Q. Simultaneous quantification of eleven bioactive components of male flowers of Eucommia ulmoides oliver by HPLC and their quality evaluation by chemical fingerprint analysis with hierarchical clustering analysis. Pharmacogn Mag 2014;10(40):435–440
16 Bai MM, Shi W, Tian JM, et al. Soluble epoxide hydrolase inhibitory and anti-inflammatory components from the leaves of Eucommia ulmoides Oliver (duzhong). J Agric Food Chem 2015;63(08):2198–2205
17 Takamura C, Hirata T, Yamaguchi Y, et al. Studies on the chemical constituents of green leaves of Eucommia ulmoides Oliv. J Nat Med 2007;61(02):220–221

18 Deyama T, Ikawa T, Kitagawa S, Nishibe S. The constituents of Eucommia ulmoides OLIV. V. Isolation of dihydroxydehydrodiconiferyl alcohol isomers and phenolic compounds. Chem Pharm Bull (Tokyo) 1987;35 (05):1785–1789
19 Hiraiwa M, Ozaki K, Yamada T, et al. mTORC1 activation in osteoclasts prevents bone loss in a mouse model of osteoporosis. Front Pharmacol 2019;10:684
20 Hu S, Wang S. The role of SIRT3 in the osteoporosis. Front Endocrinol (Lausanne) 2022;13:893678
21 Hu SJ, Cheng G, Zhou H, et al. Identification of novel cannabinoid CB2 receptor agonists from botanical compounds and preliminary evaluation of their anti-osteoporotic effects. Molecules 2022;27(03):702
22 Huang M, Wang Y, Wang Z, et al. miR-134-5p inhibits osteoclastogenesis through a novel miR-134-5p/Itgb1/MAPK pathway. J Biol Chem 2022;298(07):102116
23 Sánchez-de-Diego C, Pedrazza L, Pimenta-Lopes C, et al. NRF2 function in osteocytes is required for bone homeostasis and drives osteocytic gene expression. Redox Biol 2021;40:101845
24 Stiffel V, Amoui M, Sheng MHC, Mohan S, Lau KHW. EphA4 receptor is a novel negative regulator of osteoclast activity. J Bone Miner Res 2014;29(04):804–819
25 Tanaka T, Takahashi A, Kobayashi Y, et al. Foxf2 represses bone formation via Wnt2b/β-catenin signaling. Exp Mol Med 2022;54 (06):753–764
26 Wang Y, Jia Y, Xu Y, et al. Exploring the association between glutathione metabolism and ferroptosis in osteoblasts with disuse osteoporosis and the key genes connecting them. Comput Math Methods Med 2022;2022:4914727
27 Xuan Y, Wang J, Zhang X, et al. Resveratrol attenuates high glucose-induced osteoblast dysfunction *via* AKT/GSK3β/FYN-mediated NRF2 activation. Front Pharmacol 2022;13:862618
28 Zhang Y, Kou Y, Yang P, et al. ED-71 inhibited osteoclastogenesis by enhancing EphrinB2-EphB4 signaling between osteoclasts and osteoblasts in osteoporosis. Cell Signal 2022;96:110376
29 Zhang Y, Yang M, Zhang S, et al. BHLHE40 promotes osteoclastogenesis and abnormal bone resorption via c-Fos/NFATc1. Cell Biosci 2022;12(01):70
30 Wang S, Wang S, Wang X, et al. Effects of icariin on modulating gut microbiota and regulating metabolite alterations to prevent bone loss in ovariectomized rat model. Front Endocrinol (Lausanne) 2022;13:874849
31 Guan H, Zhao L, Cao H, Chen A, Xiao J. Epoxyeicosanoids suppress osteoclastogenesis and prevent ovariectomy-induced bone loss. FASEB J 2015;29(03):1092–1101
32 Yang S, Lin L, Chen JX, et al. Cytochrome P-450 epoxygenases protect endothelial cells from apoptosis induced by tumor necrosis factor-α via MAPK and PI3K/Akt signaling pathways. Am J Physiol Heart Circ Physiol 2007;293(01):H142–H151
33 Abshirini M, Ilesanmi-Oyelere BL, Kruger MC. Potential modulatory mechanisms of action by long-chain polyunsaturated fatty acids on bone cell and chondrocyte metabolism. Prog Lipid Res 2021;83:101113
34 Lips P, van Schoor NM. The effect of vitamin D on bone and osteoporosis. Best Pract Res Clin Endocrinol Metab 2011;25(04):585–591
35 Martini G, Mignarri A, Ruvio M, et al. Long-term bone density evaluation in cerebrotendinous xanthomatosis: evidence of improvement after chenodeoxycholic acid treatment. Calcif Tissue Int 2013;92(03):282–286
36 Epsley S, Tadros S, Farid A, Kargilis D, Mehta S, Rajapakse CS. The effect of inflammation on bone. Front Physiol 2021;11:511799
37 Lamon-Fava S, So J, Mischoulon D, et al. Dose- and time-dependent increase in circulating anti-inflammatory and pro-resolving lipid mediators following eicosapentaenoic acid supplementation in patients with major depressive disorder and chronic inflammation. Prostag Leukotr Ess 2021;164:102219
38 Robins SP, Woitge H, Hesley R, Ju J, Seyedin S, Seibel MJ. Direct, enzyme-linked immunoassay for urinary deoxypyridinoline as a specific marker for measuring bone resorption. J Bone Miner Res 1994;9(10):1643–1649
39 Chen LP, Deng MT, Chuan DU, Fang N, Luo J, Liu RH. A study of quercetin extracted from eucommia leaf promoting the proliferation of bone marrow derived mesenchymal stem cells through the phosphorylation of ERK [in Chinese]. Lishizhen Medicine and Materia Medica Research 2014;25(12):2845–2847
40 Becherini L, Gennari L, Masi L, et al. Evidence of a linkage disequilibrium between polymorphisms in the human estrogen receptor α gene and their relationship to bone mass variation in postmenopausal Italian women. Hum Mol Genet 2000;9(13):2043–2050